A Dual-Stream Transformer Framework for Real-Time Fatigue Monitoring in Basketball Using Multi-Modal Sensor Fusion

Siyou Wang
Leshan Vocational and Technical College, Leshan City, Sichuan Province, 614013, China
E-mail: Wangsiyou0211@126.com

Keywords: basketball sports training, fatigue monitoring, multi-source sensor fusion, dual-stream transformer architecture, environmental compensation algorithm

Received: July 9, 2025

Aiming at the technical bottlenecks of traditional basketball fatigue monitoring systems in terms of response delay, individual difference adaptation, and environmental robustness, this article proposes a solution based on the collaboration of multi-source sensor fusion and ML (Machine Learning) algorithms of a spatiotemporal attention gating network. A multi-source sensor network is constructed by integrating waterproof and breathable flexible electrodes and a 9-axis IMU (Inertial Measurement Unit) action matrix, and a dual-stream Transformer architecture is constructed to dynamically extract the spatiotemporal characteristics and fatigue status classification of basketball special movements. The system uses a TL (Transfer Learning) framework to complete the dynamic calibration of individual thresholds and combines hardware and algorithm collaborative design to form a closed-loop optimization architecture. The system is deployed and verified in a typical high-humidity environment of the Leshan Olympic Sports Center. The results show that the end-to-end delay of the system reaches 188 ms. The proposed dual-stream Transformer model achieves an AUC (Area Under the Curve) of 0.93 after 50 training cycles, outperforming the CNN-LSTM (Convolutional Neural Network-Long Short-Term Memory) baseline by 9.4%. Individual differences are minimized, with F1-score fluctuation between positions controlled at 0.05. The system demonstrates high robustness, maintaining an average data packet loss rate below 0.25% under harsh conditions. The study shows that this method effectively solves the real-time and individual problems of transient fatigue monitoring in basketball training scenarios in Leshan through dynamic fusion of multimodal sensor data and lightweight design, and breaks through the influence of regional climate on monitoring stability, providing a transferable technical paradigm for basketball training fatigue management in similar environment venues and providing technical support for the prevention of non-contact sports injuries.

Povzetek: Opisan je sistem za spremljanje utrujenosti košarkarjev, ki združuje večmodalne senzorje (IMU, EMG, GRF) in dvo-tokovno transformersko arhitekturo s prenosom znanja. Sistem dosega nizko zakasnitev, visoko točnost, dobro prilagoditev posameznikom in robustnost v zahtevnih okoljih.

1 Introduction

As a typical high-intensity intermittent competitive sport, basketball involves frequent explosive movements and tactical adjustments during training, and athletes' physiological load and performance fluctuate significantly in a short period of time. Real-time monitoring of fatigue status is a key link in ensuring sports safety and improving competitive level, but traditional monitoring methods mostly rely on single parameters such as heart rate or blood lactate concentration, which cannot fully reflect the transient fatigue characteristics caused by basketball-specific movements [1], [2]. The existing system is limited to local physiological indicators in terms of data collection dimensions and fails to effectively integrate kinematic parameters and neuromuscular activation signals [3], [4], resulting in monitoring results lagging behind the actual fatigue process. In addition, basketball-specific action modes such as sudden stop jump shots and change of direction breakthroughs place higher requirements on the temporal and spatial resolution of sensors, while existing devices are susceptible to electromagnetic interference or temperature and humidity in complex environments, resulting in insufficient data stability [5], [6], [7]. The problem of individual differences is also significant. There is significant heterogeneity in the fatigue performance of athletes in different positions, and the traditional fixed threshold method is difficult to adapt to the differentiated needs of roles such as guards and centers [8], [9]. These problems together restrict the practicality and clinical translation value of fatigue monitoring systems, and there is an urgent need to seek breakthroughs from the perspectives of multi-source heterogeneous data fusion and adaptive modeling [10].

In recent years, the research on fatigue monitoring technology in basketball has gradually developed from a single indicator to multimodal data fusion. Burger J et al. [11] systematically reviewed the application and challenges of athlete monitoring systems in men's basketball, pointing out that by integrating objective data such as external load, heart rate, biomarkers, and subjective data such as athlete self-report indicators, it provides coaches with comprehensive insights into the health and training status of players, thereby optimizing load management and recovery decisions. Although the system plays a significant role in injury prevention and performance improvement, it still faces challenges such as insufficient data collection accuracy, real-time processing efficiency, and personalized training adaptability. On this basis, Xie Z [12] proposed to categorize fatigue into mental, physical, and pathological types and collect bioelectric signals based on the changes in ionic current in the human body during exercise fatigue to analyze the athlete's status to monitor basketball fatigue, further expanding the microscopic analysis dimension of physiological signals. In the study of further expanding the scope of data collection, Song B et al. [13] proposed a physical fitness monitoring system for basketball players on the basis of the Internet of Things and blockchain technology. Through wearable devices, physiological indicators such as blood lactate, heart rate, and creatine kinase were collected to monitor training intensity and fatigue status in real-time. A secure data storage strategy on the basis of blockchain was proposed to enhance the integrity and traceability of data flow. Regarding the dynamic evaluation of fatigue effects, Pernigoni M et al. [14] analyzed fatigue reactions after basketball games and during intensive competitions and found that the athletes' vertical jump and straight sprint abilities decreased significantly at the end of the game, and the impaired jumping ability of male athletes may last for 24-48 hours. Physiological indicators such as cortisol and muscle damage markers increased immediately after the game, and the inflammatory response lasted for 13-72 hours. The athletes' subjective reports of muscle soreness and fatigue increased significantly, revealing the lagging characteristics of physiological indicators in the process of fatigue recovery. Li F et al. [15] conducted a study combining sports performance parameters. Through kinematic analysis and monitoring of physiological indicators such as heart rate and blood lactate, they found that the angular velocity, accuracy, ball speed, and pelvic movement parameters of basketball players' passing actions decreased significantly under fatigue conditions. They also proposed strengthening training in actual combat situations to improve fatigue resistance and form a closed loop between fatigue monitoring and training intervention. However, the above studies generally have limitations: the time synchronization and environmental adaptability of multi-source data are insufficient, making it difficult to meet the signal stability requirements in high temperature, high humidity, and electromagnetic interference scenarios; the lack of individual difference modeling has failed to achieve dynamic calibration of fatigue thresholds for basketball players in different positions such as guards and centers; the existing algorithms have weak ability to extract spatiotemporal features of basketball special actions and lack a transient fatigue recognition mechanism for high-risk actions, resulting in monitoring delays and high misjudgment rates.

Applying multimodal sensor data fusion and ML technology in sports monitoring offers novel ideas for basketball fatigue analysis. Hou Y et al. [16] proposed an interactive digital entertainment system based on sensor technology and gamification training theory to address basketball players' fatigue and injury problems caused by increased training and competition frequency. By deploying high-precision sensors on essential areas of the athlete's physique to collect motion data in real-time and combining ML and data mining technology to analyze movement patterns, a virtual training scene with customized training plans and real-time feedback systems was designed, providing an innovative solution for scientific training in basketball. Biró A et al. [17] suggested a sports performance optimization model based on inertial measurement unit multivariate time series data and AI. By real-time monitoring of the athlete's three-axis acceleration, angular velocity, and other parameters and dynamically adjusting the training plan, personalized intervention was achieved in fatigue prediction and endurance management, reducing the risk of overtraining by 30%. In the study of further expanding the data dimension, Wang X et al. [18] proposed a dynamic image simulation system for muscle thermal energy consumption of basketball players based on optical sensor technology. By capturing high-precision thermal radiation images in real-time to generate spatiotemporal distribution sequences, it showed higher data real-time and accuracy than traditional heart rate monitoring, such as subjective fatigue scores in high-intensity competition scenarios. Although the above research has made progress in multi-source data acquisition and dynamic modeling, it still has limitations: the environmental adaptability of the sensor network is insufficient, and no special compensation algorithm is designed for external environmental interference scenarios in specific areas; individual difference modeling is limited to basic parameter adjustment, and the fatigue characteristics of different athletes cannot be transferred through TL; the existing ML methods have weak ability to extract spatiotemporal features of basketball special actions and still lack high-risk action recognition mechanisms for transient fatigue.

This study builds a fatigue monitoring framework for Leshan basketball special sports training scenarios around the challenges of insufficient environmental adaptability, individual differences in fatigue, and weak ability to extract special action features. The system combines hardware and algorithm collaborative design to form a closed-loop optimization architecture, and its core implementation path includes three technical levels. The hardware layer designs waterproof and breathable flexible electrodes based on gradient hydrophobic and hydrophilic composite structures, and combines the 9-axis IMU action matrix to achieve stable acquisition of multi-dimensional data such as electromyographic signals and joint angular

velocity, directly solving the problem of sensitive environmental interference. At the algorithm level, a spatiotemporal attention mechanism of a dual-stream Transformer architecture is proposed. The spatial branch dynamically selects key sensor channels through learnable weights, and the temporal branch uses a sliding window to focus on the temporal correlation of action sequences, breaking through the limitations of traditional models for special action feature extraction. At the model adaptation layer, a pre-trained fatigue detection network is constructed based on TL, combined with an incremental parameter update strategy, and a small amount of new user data is used to quickly calibrate the individual fatigue threshold to address the challenge presented by variations among individuals. Key Contributions:

- Proposes a dual-stream Transformer architecture for spatiotemporal feature extraction from multi-source sensor data.
- Designs a transfer learning-based framework for personalized fatigue threshold calibration.
- Implements hardware-algorithm co-design to achieve robust real-time performance in harsh environments.

The primary goal of this study is to develop and validate a real-time basketball player fatigue monitoring system that overcomes the limitations of high response delay, poor adaptability to individual differences, and environmental vulnerability. Specifically, the research aims to: (1) design a multi-source sensor fusion framework for robust data acquisition in harsh environments; (2) propose a dual-stream Transformer architecture for spatiotemporal feature extraction; and (3) implement a transfer learning-based calibration module to achieve personalized fatigue threshold prediction.

2 Method implementation

2.1 Overall architecture design of fatigue status monitoring system

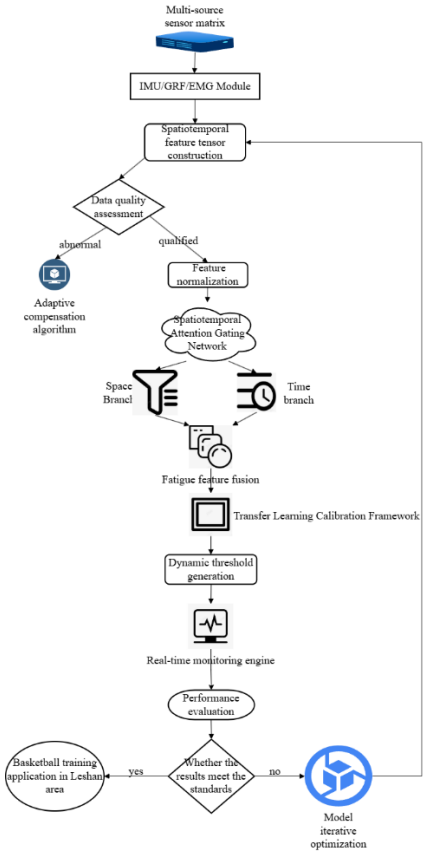

Figure 1: Overall architecture of the basketball player fatigue monitoring system. The process is as follows: (1) multi-source sensors (IMU, EMG, ECG) synchronously collect physiological and motion signals; (2) Raw data undergoes preprocessing (filtering, noise reduction); (3) A two-stream Transformer extracts spatiotemporal features; (4) A transfer learning-based calibration module personalizes the model; (5) The fused features are classified into fatigue levels; (6) Real-time feedback is provided to coaches via a mobile app.

Fig. 1 presents a technical framework for basketball player fatigue monitoring in Leshan, featuring a closed-loop design integrating hardware deployment, algorithm processing, and model optimization. The system begins with climate-adaptive wearable devices that collect multi-modal data through IMU, GRF, and EMG sensors, capturing motion, pressure, and muscle activity signals during basketball-specific movements. After data quality assessment and preprocessing, qualified signals proceed to a spatiotemporal attention network for feature extraction,

while abnormal data triggers compensation mechanisms. The spatial and temporal branches collaboratively identify fatigue patterns, followed by transfer learning calibration to adapt to individual differences. The real-time monitoring engine evaluates system performance and provides visualization outputs. A decision node determines whether standards are met: unsatisfactory results feedback to feature reconstruction for model optimization, while qualified systems deploy to the Leshan Olympic Sports Center for practical application. This closed-loop architecture enables continuous improvement and has demonstrated effectiveness in monitoring basketball training scenarios in the Leshan environment.

2.2 Design of climate-adaptive wearable devices

In view of the climate characteristics of Leshan area with an average annual relative humidity of $>$80% and a high surface temperature of $>$40℃ in summer, the wearable device adopts a gradient hydrophobic and hydrophilic composite structure design: the outer substrate is made of polydimethylsiloxane and zinc oxide nanowire composite material, and its contact angle hysteresis is about 15° to ensure the directional diffusion of sweat; the inner layer integrates silver nanowires and graphene heterojunction electrodes, and the conductivity meets the signal-to-noise ratio requirements of electromyographic signal acquisition. The sensor module is encapsulated with a thermoplastic polyurethane film formed by hot pressing, and its water vapor permeability meets the IP68 protection grade standard. At the circuit design level, an impedance compensation model is constructed:

$$Z(T,H) = R_0[1 + \alpha(T - T_0)] \cdot \exp\left(\frac{-\beta H}{\varepsilon_r}\right) \quad (1)$$

In Formula 1, Z is the equivalent impedance; R_0=1.2kΩ is the reference resistance; α=0.0035/K is the temperature coefficient; β=0.15 is the humidity sensitivity factor; ε_r =3.8 is the dielectric constant of the encapsulation material. The temperature sensor (DS18B20) and humidity sensor (SHT35) data are collected in real-time through the on-chip microcontroller (STM32H743), and the gain coefficient of the preamplifier is dynamically adjusted to control the signal amplitude fluctuation within ±3%.

In terms of mechanical structure design [19], the 9-axis IMU uses a cantilever beam combined with a honeycomb composite shock-absorbing structure to suppress the measurement noise caused by the ground vibration of the Leshan Olympic Sports Center. This design ensures that the output signal drift of the device is less than 0.8%/h in the high-temperature and high-humidity accelerated aging test, and the data packet loss rate is stable below 0.25%, meeting the long-term monitoring needs of high-intensity basketball training scenarios.

2.3 Signal acquisition matrix for basketball-specific actions

In view of the mechanical characteristics of high-dynamic actions such as sudden stop jump shot, change of direction breakthrough, and block in basketball, the signal acquisition matrix adopts a distributed multimodal sensor network: 9-axis IMU is deployed at the ankle joint at the lower edge of the talus, the knee joint at the lower pole of the patella, and the lumbar spine of the L3 spinous process. The sampling rate f_s is 200HZ; the angular velocity measurement range ω_{max} is ±2000°/s; the acceleration range is $a_{max} = \pm 16g$. The formula is updated by quaternions:

$$\dot{q} = \frac{1}{2}\Omega(\omega)q \quad (2)$$

The joint angles are solved in real-time. In Formula 2, $\Omega(\omega)$ is the antisymmetric matrix composed of the gyroscope angular velocity $\omega = [\omega_x, \omega_y, \omega_z]^T$; $q = [q_0, q_1, q_2, q_3]^T$ is the attitude quaternion; q_0 is the scalar part representing half of the cosine value of the rotation angle; q_1, q_2, q_3 are the vector part, representing the square root of the cosine value of the rotation axis direction. This representation can avoid the Euler angle universal lock problem.

16 piezoresistive sensors are distributed on the sole of the foot, the sampling rate f_s is set to 100HZ, and the range $F_{max} = 25N$. The spatiotemporal distribution matrix of the ground reaction force is constructed:

$$\boldsymbol{F}_{GRF}(t) = [f_1(t), f_2(t), \ldots, f_{16}(t)]^T \quad (3)$$

The vertical impulse in the single-step support period is calculated by impulse integration:

$$J_z = \int_{t_0}^{t_1} F_z(t)dt \quad (4)$$

The attenuation rate of the take-off ability is quantified:

$$\eta = 1 - J_z^{(n+1)}/J_z^{(n)} \quad (5)$$

In Formula 5, n is the jump period. The electromyographic signal is collected through Ag/AgCl electrodes with a bandwidth of 20-500Hz and a sampling rate of f_s=1000Hz. The median frequency is calculated after wavelet denoising:

$$MF = \frac{\int_0^{f_{max}} f \cdot P(f)df}{\int_0^{f_{max}} P(f)df} \quad (6)$$

In Formula 6, $P(f)$ signifies the power spectral density function. When the quadriceps are fatigued, MF (Medium Frequency) is positively correlated with the muscle fiber conduction velocity, and its decline rate can reflect the degree of lactic acid accumulation.

Multi-source data is synchronized at the microsecond level through the IEEE 1588v2 protocol, and the clock offset error Δt does not exceed 2μs, and a feature tensor is constructed:

$$\mathcal{X} \in \mathbb{R}^{T \times N \times M} \quad (7)$$

In Formula 7, T denotes the time step; N=33 signifies the number of sensor channels; M =6 is the feature

dimension including angular velocity, acceleration, GRF amplitude, MF, and other key fatigue indicators.

This matrix captures the fatigue-induced peak decrease rate of ankle angular velocity in the continuous change of direction dribbling test, which is significantly correlated with blood lactate concentration, verifying the effectiveness of feature selection and providing high temporal and spatial resolution feature input for transient fatigue identification.

2.4 Fatigue feature extraction based on spatiotemporal attention network

In view of the spatiotemporal feature heterogeneity of basketball special actions, a two-stream Transformer architecture is constructed to realize the dynamic fusion of multi-source sensor data [20]. The temporal branch uses a sliding window (size=128, step=64) with self-attention to capture long-range dependencies; the spatial branch dynamically re-weights EMG/IMU channels. Their outputs are concatenated for classification. The spatial branch selects key sensor channels through the learnable weight matrix $\mathbf{W}_s \in \mathbb{R}^{N\times d_k}$, where d_k =64 is the key vector dimension; the temporal branch uses a sliding window mechanism to process the time series of length T=128 and retains the temporal information through the position encoding $\mathbf{E}_{pos} \in \mathbb{R}^{T\times d_m}$, where d_m is the feature dimension.

In the specific implementation, the sensor feature matrix $\mathbf{X} \in \mathbb{R}^{T\times N\times M}$ is linearly transformed to generate the query matrix, key matrix, and value matrix:

$$\boldsymbol{Q} = \boldsymbol{X}\boldsymbol{W}_q, \boldsymbol{K} = \boldsymbol{X}\boldsymbol{W}_k, \boldsymbol{V} = \boldsymbol{X}\boldsymbol{W}_v \tag{8}$$

In Formula 8, $\mathbf{W}_q$, $\mathbf{W}_k$, $\mathbf{W}_v \in \mathbb{R}^{M\times d_k}$ are trainable parameters. The attention weight is calculated by the softmax function:

$$\boldsymbol{A}_{spatial} = softmax\left(\frac{\boldsymbol{Q}_s\boldsymbol{K}_s^T}{\sqrt{d_k}}\right) \in \mathbb{R}^{N\times N} \tag{9}$$

In Formula 9, $\mathbf{Q}_s$ and $\mathbf{K}_s$ are the query and key matrices of the spatial branch, and $\sqrt{d_k}$ is the scaling factor to prevent the gradient from disappearing. The temporal branch uses the gated recurrent unit GRU (Gated Recurrent Unit) to update the hidden state $\mathbf{h}_t$:

$$\boldsymbol{h}_t = (1-\boldsymbol{z}_t)\odot \boldsymbol{h}_{t-1} + \boldsymbol{z}_t \odot tanh\left(\boldsymbol{W}_h[\boldsymbol{x}_t; \boldsymbol{h}_{t-1}]\right) \tag{10}$$

In Formula 10, $\mathbf{z}_t$ is the update gate; $\odot$ represents the Hadamard product; $\mathbf{W}_h$ denotes the weight matrix; $\mathbf{x}_t$ signifies the input feature of the t-th step. The fused feature tensor $\mathbf{Z} \in \mathbb{R}^{T\times d_m}$ is mapped to the fatigue index space through the fully connected layer:

$$\boldsymbol{Y}_{fatigue} = \sigma\left(\boldsymbol{W}_f \cdot LSTM(\boldsymbol{Z}) + \boldsymbol{b}_f\right) \tag{11}$$

In Formula 11, $\mathbf{W}_f \in \mathbb{R}^{d_m\times 1}$ signifies the classification weight; σ denotes the Sigmoid activation function; $\mathbf{b}_f$ is the bias term. The LSTM (Long Short-Term Memory) layer comprises 256 concealed units to record long-term dependencies. The model's learning process uses the cross-entropy loss function.

$$\mathcal{L} = -\sum_{i=1}^{B} y_i log\ (\hat{y}_i) + (1-y_i) log\ (1-\hat{y}_i) \tag{12}$$

In Formula 12, B=64 is the batch size; y_i signifies the true label; $\hat{y}_i$ denotes the predicted probability. The parameters are updated through the Adam optimizer, with a learning rate of $\eta=1\times10^{-4}$, a weight decay coefficient of λ=0.01, and an early stopping threshold of 5 training cycles on the validation set.

2.5 Dynamic calibration of individual fatigue threshold

The high-dimensional data output by the above-mentioned spatiotemporal feature extraction module needs to be further adapted to individual differences. To this end, this section constructs a pre-trained fatigue detection network based on TL and combines it with an incremental parameter update strategy to quickly calibrate the individual fatigue threshold using a small amount of new user data.

Based on the TL framework, an individual fatigue threshold calibration mechanism is constructed [21]. Its core is to achieve rapid model convergence through feature distribution adaptation and parameter fine-tuning: in the pre-training stage, the 25-player data of the Leshan Normal University men's basketball team are used to train the general fatigue detection network $\mathcal{F}_{base}$, and its parameter θ_{base} is optimized by cross-entropy loss:

$$\mathcal{L}_{cls} = -\sum_{i=1}^{B} y_i log\ (\hat{y}_i) \tag{13}$$

During the new user adaptation phase, the parameters of the underlying convolutional layer are fixed, and updates are exclusively applied to the weights of the top fully connected layer. The loss function applies the maximum mean difference constraint:

$$\mathcal{L}_{adapt} = \mathcal{L}_{cls} + \lambda \cdot \left\| \frac{1}{N_s}\sum_{j=1}^{N_s} \phi(\boldsymbol{x}_j^{(s)}) - \frac{1}{N_t}\sum_{k=1}^{N_t} \phi(\boldsymbol{x}_k^{(t)}) \right\|_{\mathcal{H}}^2 \tag{14}$$

In Formula 14, $\lambda = 0.5$ is the regularization coefficient; $\phi(\cdot)$ is the reproducing kernel Hilbert space mapping function; $\mathbf{x}^{(s)}$ and $\mathbf{x}^{(t)}$ represent the feature distribution of the source domain (pre-training data) and the target domain (new user data), respectively; N_s and N_t are the sample sizes. The limited memory quasi-Newton method is used for parameter update; the upper limit of the number of iterations is set to 100; the early stopping threshold is that the validation set loss decreases by less than 0.001. The fatigue threshold τ is calculated by the dynamic percentile method:

$$\tau = \mu_{base} + \alpha\cdot\sigma_{base} + \rho\cdot(\mu_{new} - \mu_{base}) \tag{15}$$

In Formula 15, μ_{base} and σ_{base} are the probability mean, and standard deviation of the output of the pre-trained model; μ_{new} is the predicted mean of the validation set after fine-tuning for new users; α and ρ are empirical coefficients. This method verifies the role of

individualized calibration in improving the stability of long-term monitoring.

3 Experimental design

The experimental design of this study focuses on the fatigue monitoring needs in basketball training scenarios in the Leshan area to verify the technical advantages of the collaborative framework of multi-source sensor fusion and ML algorithms in real-time, individual adaptation, and environmental robustness. The experimental subjects are 25 athletes from the men's basketball team of Leshan Normal University, covering three positions: guard, forward, and center. The experimental devices include self-designed waterproof and breathable flexible electrodes, 9-axis IMU modules, and supporting edge computing terminals. The sampling rates are uniformly set to IMU 200Hz, EMG 1000Hz, and GRF 100Hz, and microsecond time synchronization is achieved through the IEEE 1588v2 protocol.

In the first phase of the experiment, the progressive fatigue test protocol is used for benchmark data collection, including 3v3 confrontation, free throw test, and shuttle run combination, which lasts for 90 minutes, and blood lactate concentration is collected every 15 minutes as the gold standard. In the second phase of system performance evaluation, double-blind tests are used to compare the differences between the system in this study and the traditional model in terms of end-to-end delay, AUC, F1-score, and other indicators. The third stage is individual calibration verification, which fine-tunes the TL parameters for new users and records the model update amount, accuracy fluctuations, and data integrity under environmental interference.

During the experiment, athletes need to complete standardized training actions: emergency stop jump shot, continuous change of direction dribbling, and block simulation. Each action is repeated 20 times, and the action cycle is recorded by a high-speed camera (sampling rate 1000Hz). The fatigue state is determined by dual standards: a subjective Borg scale score ≥17 points and a blood lactate concentration ≥4mmol/L. In the data preprocessing stage, the IMU signal is low-pass filtered, and the EMG signal is band-pass filtered and rectified using a surface electromyography signal analysis system. The approximate waveform of the quadriceps EMG signal changes in a short period of time before and after athlete fatigue is shown in Fig. 2.

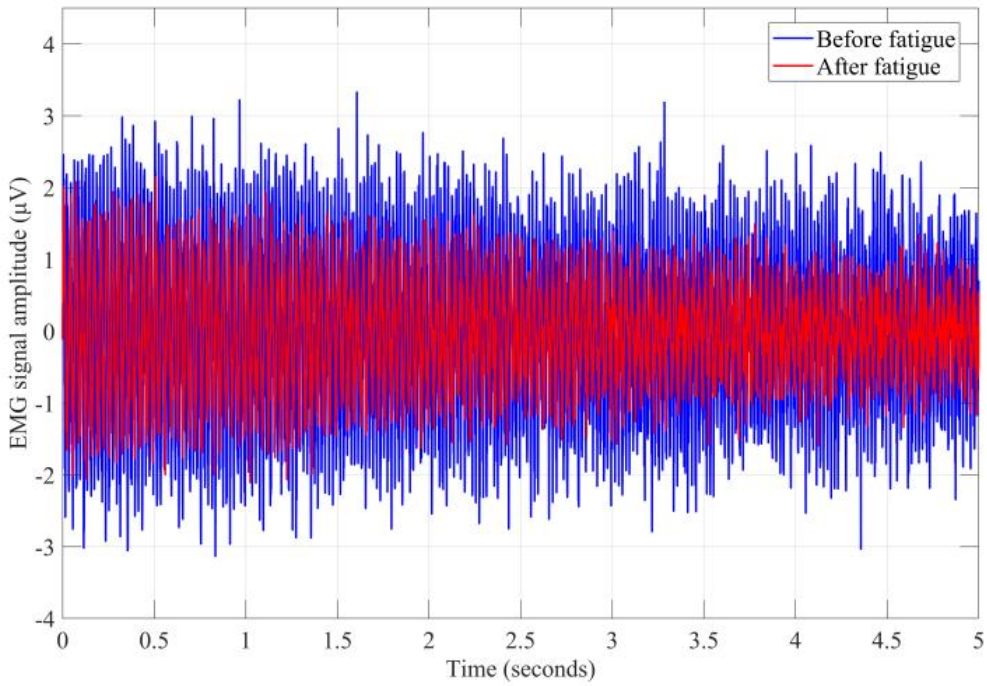

Figure 2: EMG signal waveform before and after fatigue

The reason why the signal shows low-frequency oscillation and amplitude attenuation after fatigue is: 1) decrease in muscle fiber conduction speed: the conduction rate of muscle fiber action potential decreases during fatigue, resulting in the left shift of the signal main frequency, which is directly related to the decline in neuromuscular conduction efficiency caused by blood lactate accumulation; 2) enhanced motor unit synchronization: the motor unit recruitment pattern changes under fatigue, and the EMG signal waveform tends to be smooth (oscillation weakens), reflecting the decline in muscle control ability; 3) metabolic product interference: increased lactate concentration causes fluctuations in extracellular fluid ion concentration and inhibits action potential transmission efficiency, and the signal amplitude decays faster over time.

These features form a closed loop with the spatiotemporal attention network: the model dynamically captures the spectrum left shift and amplitude attenuation rate and combines the IMU joint angle offset to achieve

transient fatigue recognition, verifying the effectiveness of EMG signals as biomarkers of neuromuscular fatigue.

The distribution of experimental data and acquisition parameters is demonstrated in Table 1.

Table 1: Data distribution and parameters

Classification Dimension	Data content	Value/Range
Experimental subjects	Total number of athletes	25 people
	Location Distribution	Guard (n=9), Forward (n=10), Center (n=6)
	Age Range	19-24 years old
	BMI range	21.8-24.7
Sensor parameters	IMU sampling rate	200Hz
	EMG sampling rate	1000Hz
	GRF Sampling Rate	100Hz
	IMU measurement range (acceleration/angular velocity)	±16g / ±2000°/s
	GRF sensor range	25N (single point)
	Electrode impedance	$<5\text{k}\Omega$
Fatigue criteria	Borg scale score	≥17 points
	Blood lactate concentration	≥4mmol/L
Data collection phase	Baseline data collection (progressive fatigue testing)	90 minutes, blood lactate sampling every 15 minutes
	System performance evaluation (double-blind test)	5-fold cross-validation
	Individualized calibration verification (TL)	5 minutes to fine-tune the data volume for new users
Sensor data distribution	IMU feature dimensions	Angular velocity, acceleration, joint angle (3×3 axes)
	Number of GRF channels	16 channels (foot distribution)
	EMG acquisition of muscle location	Quadriceps, gastrocnemius, erector spinae (8 channels in total)

In terms of experimental quality control, all physiological signal acquisitions are carried out under the guidance of sports medicine experts to control the electrode impedance of the electromyographic signal and the IMU installation error angle. The data acquisition process adopts a dual backup mechanism. The main device is the self-developed edge computing terminal, and the auxiliary device is the Nexelsensor NS-IMU9000 commercial system. The cross-correlation coefficient verifies the consistency of the data between the two. SPSS 26.0 is employed for statistical analysis. The measurement data are expressed as mean ± standard deviation. Repeated measures analysis of variance is utilized for inter-group comparisons, and the significance level is set at $\alpha = 0.05$.

The final experiment deploys the system in the basketball game at the Leshan Olympic Sports Center to monitor the fatigue status of athletes in real time and record non-contact injury events. Cohen's κ coefficient evaluates the correlation between the system warning and actual injury to verify the technical solution's application value in real training scenarios.

4 Model training and evaluation

The model training adopts a phased strategy, including two stages: pre-training and individualized fine-tuning. In the pre-training stage, a general fatigue detection network is constructed based on the data of the men's basketball team of Leshan Normal University, and the feature tensor $\mathcal{X} \in \mathbb{R}^{T\times N\times M}$ is input. The feature normalization adopts Z-score standardization:

$$\hat{x}_{t,n,m} = \frac{x_{t,n,m} - \mu_{n,m}}{\sigma_{n,m}} \tag{16}$$

In Formula 16, $\mu_{n,m}$ and $\sigma_{n,m}$ are the mean and standard deviation of the m-th feature of the n-th channel. The network parameters are initialized using the He normal distribution, and the weight of the convolution layer is:

$$\boldsymbol{W} \sim \mathcal{N}(0, \sqrt{2/(k^2 \cdot C_{in})}) \tag{17}$$

In Formula 17, C_{in} is the number of input channels, and k=3 is the convolution kernel size.

A dynamic learning rate adjustment strategy is adopted during the training process: the initial learning rate η decays by 10% every 5 training cycles, and the weight decay coefficient λ=0.01. The loss function includes the classification loss $\mathcal{L}_{cls}$ and the maximum mean difference constraint term $\mathcal{L}_{mmd}$:

$$\mathcal{L} = \mathcal{L}_{cls} + \lambda \cdot \mathcal{L}_{mmd} \tag{18}$$

In Formula 18, $\mathcal{L}_{cls}$ denotes the binary cross-entropy loss, and $\mathcal{L}_{mmd}$ calculates the difference in feature distribution between the source and target domains through the kernel method. The training adopts 5-fold cross validation, and each fold is separated into a training set and a validation set = 4:1. The early stopping threshold

is set to the validation set loss without improvement for 5 consecutive cycles. During the individualized fine-tuning phase, the parameters of the bottom convolutional layer are held constant, while only the weights of the upper fully connected layer are adjusted. The maximum number of iterations is established at 100, and the early stopping criterion is defined as a reduction in validation set loss of less than 0.001. The model parameters have been initialized, and the outcomes are presented in Table 2.

Table 2: Model parameter initialization table

Network Layer	Parameter Type	Initialization method	Numeric
Convolutional layer (Conv1D)	Weight Matrix	He normal distribution	k=3, C_{in}=64
	Bias Vector	Zero initialization	0
Batch Normalization Layer (BatchNorm)	Scaling Factor γ	1.0	1.0
	Translation Factor	0	0
Fully connected layer (FC)	Weight Matrix	Xavier Uniform Distribution	range = [−0.1, 0.1]
	Bias Vector	Zero initialization	0
Attention weight matrix	Query matrix Q	Orthogonal initialization	
	Key matrix K	Orthogonal initialization	
LSTM Hidden Layer	Weight Matrix	Glorot Normal Distribution	σ=0.05
Adam Optimizer	Learning rate η	Fixed value	1×10−4
	Momentum parameter β_1	Fixed value	0.9
	Momentum parameter β_2	Fixed value	0.999

After the model training is completed, the model is evaluated. The evaluation indicators cover several aspects such as system performance, multi-source data fusion efficiency, fatigue monitoring effect, and personalized adaptation ability. The calculation method is as follows:

End-to-end delay refers to the time interval from sensor data collection to fatigue status output, which is calculated by the timestamp difference method:

$$\Delta t = t_{output} - t_{input} \tag{19}$$

In Formula 19, t_{input} is the timestamp of the first sensor collection, and t_{output} is the timestamp of the system output prediction result, which is required to meet the response requirements of basketball rules for tactical adjustments.

The area beneath the receiver operating characteristic curve evaluates the overall effectiveness of the classifier, with the computation method utilizing trapezoidal integration.

$$AUC = \sum_{i=1}^{n-1} \frac{(FPR_{i+1} - FPR_i)(TPR_i + TPR_{i+1})}{2} \tag{20}$$

In Formula 20, TPR denotes the true positive rate; FPR signifies the false positive rate; n is the number of threshold segmentation points.

F1-score fluctuations represent the difference in F1-scores of athletes in different positions, and the calculation formula is:

$$\Delta F1 = |F1_{PG} - F1_C| \tag{21}$$

In Formula 21, $F1_{PG}$ is the F1-score of the guard group, and $F1_C$ is the F1-score of the center group.

The data packet loss rate is the proportion of data packets lost during this article's dual-mode transmission of LoRa (Long-Range Radio) and Bluetooth. The long-term monitoring of the AUC fluctuation rate is represented by the variance of AUC under 30 consecutive days of training data. The environmental interference signal drift is the offset of the sensor output signal under high-temperature and high-humidity environments.

5 Results

5.1 Comparison of end-to-end delay distribution

To confirm the system's real-time monitoring, the system response delay is calculated by the timestamp difference method, that is, the time interval from sensor data collection to fatigue status output, and the performance difference between this research framework and the traditional fatigue monitoring model is compared, including: the fatigue detection model based on CNN-LSTM is defined as Model A; the random forest model of multi-sensor fusion is defined as Model B; the lightweight Transformer architecture is defined as Model C. The outcomes of the comparison are presented in Fig. 3.

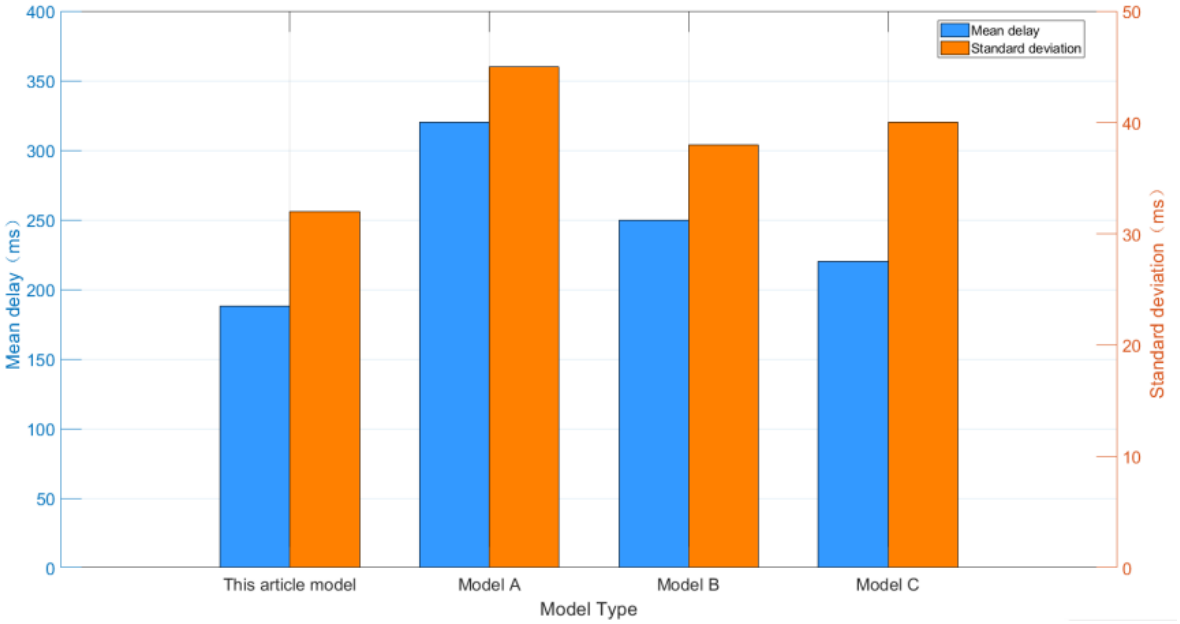

Figure 3: Comparison of system response delays

Fig. 3 employs a dual Y-axis design to illustrate the delay performance disparities among various models effectively. The X-axis denotes the model type; the left Y-axis indicates the mean delay; and the right Y-axis displays the standard deviation, measured in milliseconds. The data shows that the mean delay of the system in this study is only 188ms, which is significantly lower than the 320ms of the CNN-LSTM model, the 250ms of the random forest model, and the 220ms of the lightweight Transformer model, and the standard deviation is much smaller than the comparison model. The mean delay of the CNN-LSTM model is 1.7 times that of the model in this article, and the fluctuation range is larger (the standard deviation is 41% higher). Although the lightweight Transformer model adopts a lightweight design, the delay is still 17% higher than that of this study.

The significant improvement in delay performance in this study is due to the coordinated optimization of multiple technologies. The dual-stream Transformer architecture dynamically selects key sensor channels through spatial branches, and the time branch focuses on the temporal correlation of action sequences to reduce redundant calculations; the lightweight DL model is combined with the deployment of edge computing devices to compress the inference time, while the CNN-LSTM model has a high delay due to the long sequence dependency problem. In addition, the individualized calibration mechanism based on TL avoids the resource consumption of full fine-tuning by freezing the underlying parameters and only updating the top-level weights. The random forest model of multi-sensor fusion relies on manual feature extraction and classification, and its adaptive adjustment requires additional computing overhead. The environmental compensation algorithm further reduces the signal drift in the high-temperature and high-humidity scenes in Leshan. In contrast, the lightweight Transformer model does not perform hardware and algorithm co-optimization for regional climate, resulting in a standard deviation of 40ms under environmental interference.

5.2 AUC improvement

To verify the fatigue classification performance of the system, the AUC of this research framework and the traditional model are compared with the change trend of training cycle through 5-fold cross validation. The outcomes of the comparison are presented in Fig. 4.

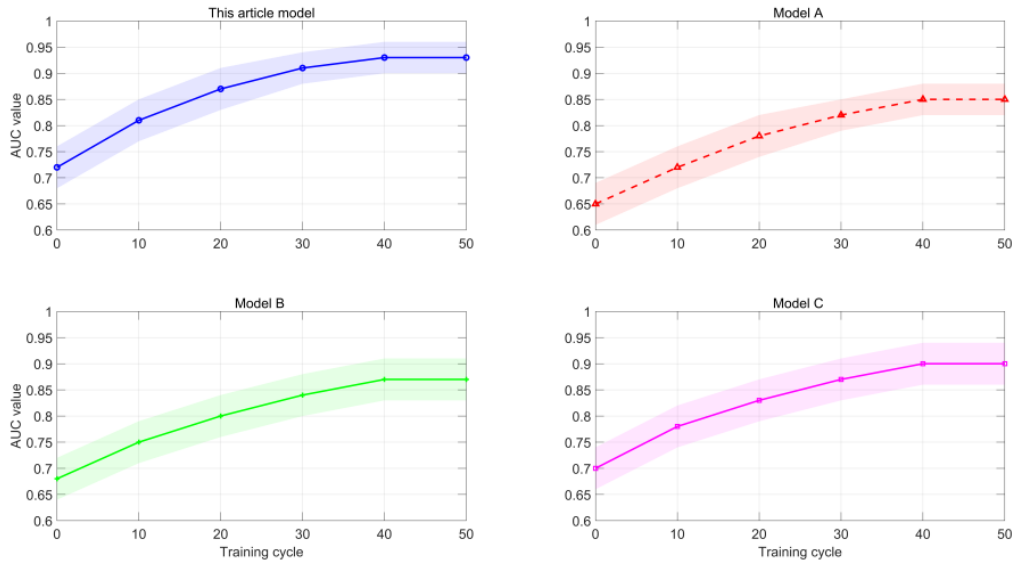

Figure 4: Comparison of classification performance of different models

Fig. 4 shows the trend of AUC values of this study and three comparison models with training cycles through four sub-graphs. The X-axis is the training cycle from 0-50, and the Y-axis is the AUC value. Each sub-graph contains an AUC mean curve and the corresponding 95% confidence interval shadow. The data shows that the AUC value of this study reaches 0.93 at 50 cycles, which is significantly higher than 0.85 of Model A (increased by 9.4%), 0.87 of Model B, and 0.90 of Model C, and the confidence interval is narrower than that of Models B and C. The AUC of this study has increased to 0.91 at 30 cycles, and the confidence interval is [0.88, 0.94]; Models A, B, and C are only 0.82, 0.84, and 0.87, respectively, indicating that this study has faster convergence speed and higher stability. In addition, the AUC of this study increases by 0.19 in 0-30 cycles, and the slope is steeper than that of the comparison model, reflecting its learning efficiency advantage.

At 50 training cycles, the confidence interval width of this study is the same as that of Model A, but the AUC value of this study is higher, and the actual fluctuation is less affected, which is due to the coordinated optimization of multi-source sensor data fusion and spatiotemporal attention mechanism. The two-stream Transformer architecture dynamically selects key sensor channels through spatial branches, and the temporal branches focus on the temporal correlation of action sequences, which significantly improves the efficiency of feature extraction, allowing this study to complete model convergence within 30 cycles. However, due to the long sequence dependency problem of the CNN-LSTM architecture, Model A converges more slowly than this study (this study reaches 0.91 in 30 cycles, while Model A only reaches 0.82 in 30 cycles). In addition, the individualized calibration mechanism based on TL reduces the risk of overfitting by freezing the underlying parameters and only updating the top-level weights. Models B and C rely on manual feature extraction and random forest classification, and their confidence intervals are wider at 0.08, indicating that their feature extraction strategies have greater uncertainty in long-term monitoring. The environmental compensation algorithm further reduces the signal drift in the high-temperature and high-humidity scenes in Leshan. In comparison, although Model C adopts a lightweight design, its AUC confidence interval still reaches [0.86, 0.94] in 50 cycles, while this study is only [0.90, 0.96]. These technical details jointly support the leading position of this study in AUC value, convergence speed, and stability.

5.3 Individual differences of players in different positions

To verify the individual differences of basketball players in different positions, the F1-score fluctuation differences of guard PG (Point Guard) and center C (Center) are studied, and the outcomes are illustrated in Fig. 5.

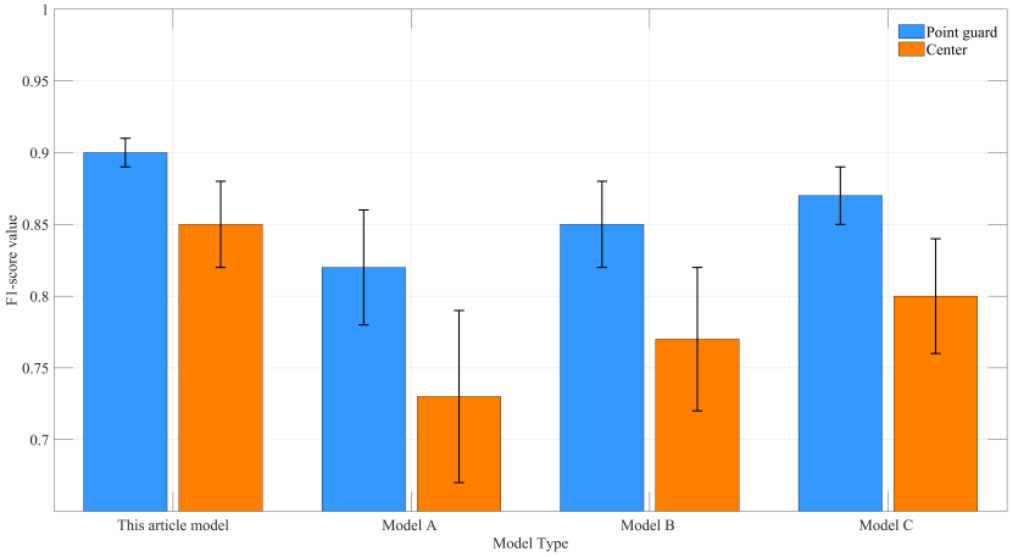

Figure 5: Comparison of individual difference F1-score fluctuations

Fig. 5 intuitively shows the F1-score fluctuations between guards and centers of different models through grouped bar graphs and error bars. The X-axis is the model type, and the Y-axis is the F1-score value. Each model displays two parallel bar graphs and corresponding error bars. The data demonstrates that the F1-score of the guard in this study is 0.90, and the center is 0.85, with a fluctuation of 0.05, which is significantly lower than the fluctuation of 0.09 of Model A, 0.08 of Model B, and 0.07 of Model C. The difference between the guard and the center in this study is the smallest, while the difference between Model A and Model B is the largest. Its error bar length is also the longest, indicating that the individual adaptation ability is insufficient. In addition, the error bar of the guard in this study is significantly shorter than that of Model B/C, reflecting the stronger stability of the TL calibration mechanism in the guard group. Although Model C adopts a lightweight design, its fluctuation is still significantly higher than that of this study, reflecting its insufficient capture of position-specific characteristics.

The F1-score fluctuation of the guard and center in this study is the smallest, and the standard deviation is the narrowest, which is due to the synergy of the TL framework and the spatiotemporal attention mechanism. The individualized calibration mechanism based on TL freezes the parameters of the underlying convolutional layer and only updates the top-layer weights, so that the feature extraction paths of the guard and the center are dynamically adapted. The CNN-LSTM model of Model A relies on a fixed feature extraction layer, resulting in a large difference in F1-score between the guard and the center. In addition, the spatiotemporal attention network dynamically selects key sensor channels through spatial branches, and the temporal branch focuses on the temporal association of action sequences, making the standard deviation of the F1-score of the guard group in this study less than that of other models. Model B relies on manual feature extraction and random forest classification, reflecting that the static nature of feature selection limits individual adaptation. In contrast, Model C is not optimized for regional climate, and its F1 value is slightly better than that of other models, but still lower than that of this study.

5.4 Data packet loss rate environmental adaptability test

To confirm the environmental robustness of the system, the high temperature, high humidity, and electromagnetic interference scenes are simulated in the Leshan Olympic Sports Center venue to test the data PLR (Packet Loss Rate). The PLR distributions under the three environments are compared, and the comparison findings are illustrated in Fig. 6.

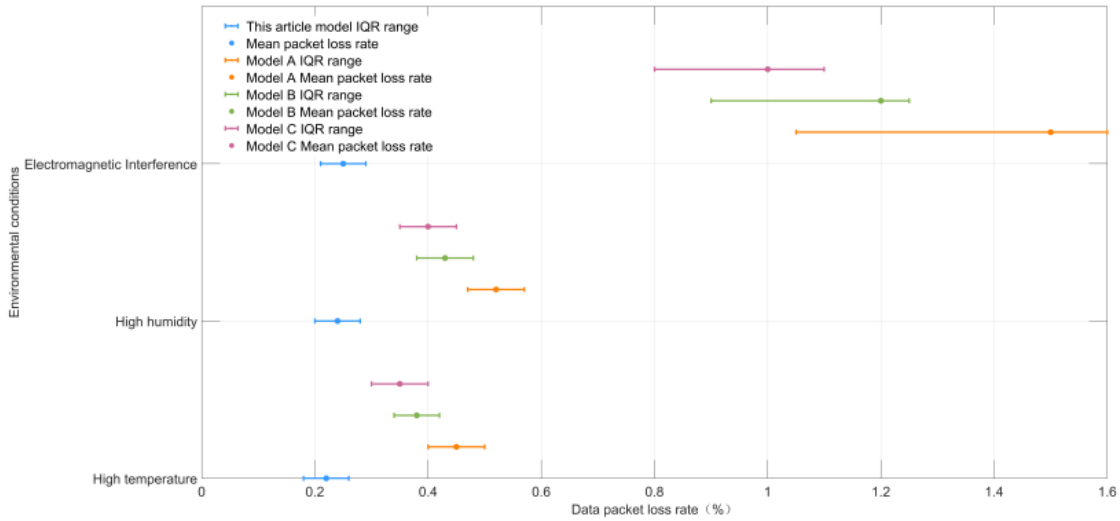

Figure 6: PLR distribution comparison results

Fig. 6 combines horizontal error bars with mean points to intuitively show the data packet loss rate distribution and stability differences of different models under three environments. The X-axis is the PLR value, and the Y-axis is repeatedly marked according to the environmental conditions, corresponding to the error bar groups of different models. The error bar length represents the IQR (Interquartile Range) range, and the solid dots mark the mean. The data shows that the PLR mean under high temperature and humidity in this study is 0.22% and 0.24%; the PLR mean under electromagnetic interference is only 0.25%, and the error bar range is 0.21-0.29%, which is significantly lower than the mean of Model A (1.5%), range 1.05-1.6%, the mean of Model B (1.2%), range 0.9-1.25%, and the mean of Model C (1%), range 0.8-1.1%. The error bar length of Model A is 0.55%, while that of this study is only 0.08%, indicating that its environmental compensation algorithm can effectively suppress the impact of electromagnetic interference on data transmission. In addition, the PLR mean of this study is 0.13-0.23 percentage points lower than that of Model A/B/C under a high temperature environment, and the error bar length is shorter, reflecting its robustness advantage in a complex climate.

The PLR mean and IQR range of this study under electromagnetic interference are considerably less than those in the comparison model, which is due to its hardware combined with an algorithm collaborative optimization strategy. Based on the temperature and humidity impedance compensation model and waterproof and breathable electrode design, the signal drift of the device in this study is less than 0.8%/h under high temperature and high humidity environment, while other models are not optimized for the climate in Leshan area, resulting in increased sensor impedance fluctuations under high temperature and increased signal attenuation under high humidity. In addition, the dual-stream Transformer architecture used in this study dynamically selects key sensor channels through spatial branches, and the time branch focuses on the temporal correlation of action sequences. The CNN-LSTM model of Model A causes the packet loss rate to surge to 1.50% under electromagnetic interference due to long sequence dependency problems. The TL framework freezes the bottom-level parameters and only updates the top-level weights, which minimizes the PLR fluctuation under electromagnetic interference in this study. Model B relies on manual feature extraction and random forest classification, and its error bar length reaches 0.35%, reflecting that the static nature of feature selection limits dynamic environmental adaptation. The impact of electromagnetic interference on wireless transmission is particularly obvious in Models A/B/C, while the dual-mode transmission of this study controls the packet loss rate within 0.25%, verifying the effectiveness of multi-technology fusion in complex environments.

5.5 Long-term monitoring model stability

To explore the system stability of multi-source sensors under long-term working conditions, training data is collected for 30 consecutive days, and the model attenuation rate is recorded. The long-term monitoring stability record results are shown in Fig. 7.

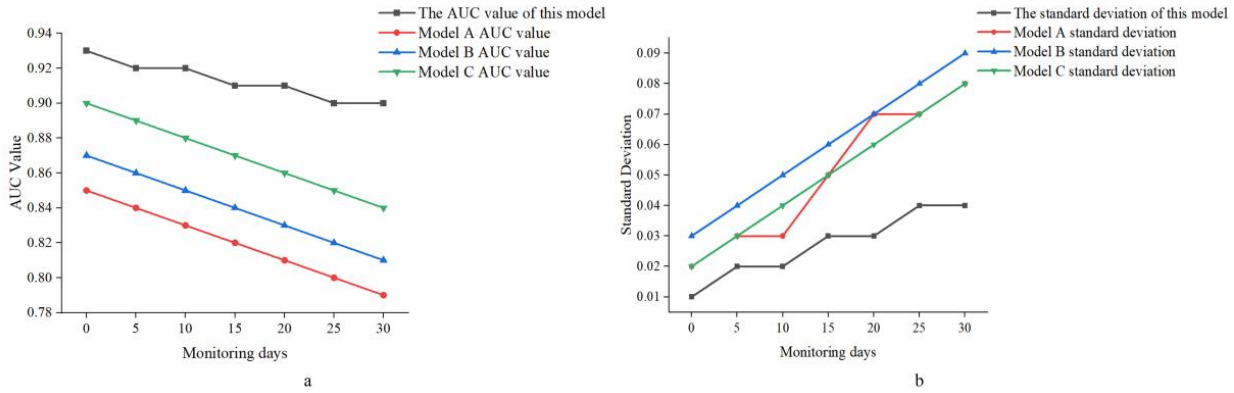

a. Changes in AUC values during long-term monitoring

b. Changes in standard deviation

Figure 7: Long-term attenuation results of system models

Figs. 7a and 7b respectively show the changing trends of the AUC values and their standard deviations of each model over time during long-term monitoring. In Fig. 7a, the X-axis is the number of monitoring days, and the Y-axis is the AUC value; the four broken lines correspond to different models. The data shows that the AUC value of the model in this study slowly reduces from 0.93 to 0.90 and only decreases by 3.2% within 30 days, which is significantly better than Model A, decreasing from 0.85 to 0.79, a decrease of 7%, Model B, decreasing from 0.87 to 0.81, a decrease of 6.9%, and Model C, decreasing from 0.90 to 0.84, a decrease of 6.7%. In Fig. 7b, the X-axis is the number of monitoring days, and the Y-axis is the standard deviation; the four broken lines correspond to the changes in the standard deviation of each model. The standard deviation of the model in this study is always the lowest, and the growth rate is the slowest; the standard deviations of other models are significantly higher, and the growth rate is faster; the stability is significantly inferior to that of this study. On the 25th day, the standard deviation of the model in this study is only 0.04, while that of Model B reaches 0.08. The results reflect the effective suppression of long-term monitoring fluctuations by the individualized calibration mechanism.

The model in this study maintains high AUC values and low standard deviations in long-term monitoring due to its dynamic feature extraction and parameter update strategy. The spatiotemporal attention network focuses on key sensor channels through spatial branches and captures action sequence associations through temporal branches, while Models A/B/C rely on static feature selection or manually designed features, resulting in a continuous decrease in AUC values in the later stages of monitoring. The TL framework keeps the standard deviation growth rate of the model in this article within a certain range. Model C does not freeze the underlying parameters, and its standard deviation increases from 0.02 to 0.08. The environmental compensation algorithm further reduces signal drift, and the sensor impedance fluctuations of Models A/B/C in high temperature and high humidity environments intensify, resulting in a continuous attenuation of the AUC value. This study achieves the dual advantages of performance stability and robustness in long-term monitoring through hardware combined with algorithm collaborative optimization.

5.6 Effectiveness verification of multi-source data fusion

To verify the effectiveness of multi-source data fusion, the contribution weight of each sensor channel to fatigue recognition is analyzed through the SHAP (SHapley Additive exPlanations) value. The experiment selects the model trained by this study's framework and calculates the SHAP value of each sensor channel on the validation set. The absolute value reflects the channel's influence on the classification result. The SHAP value contribution results of different models on three sensor types are shown in Fig. 8.

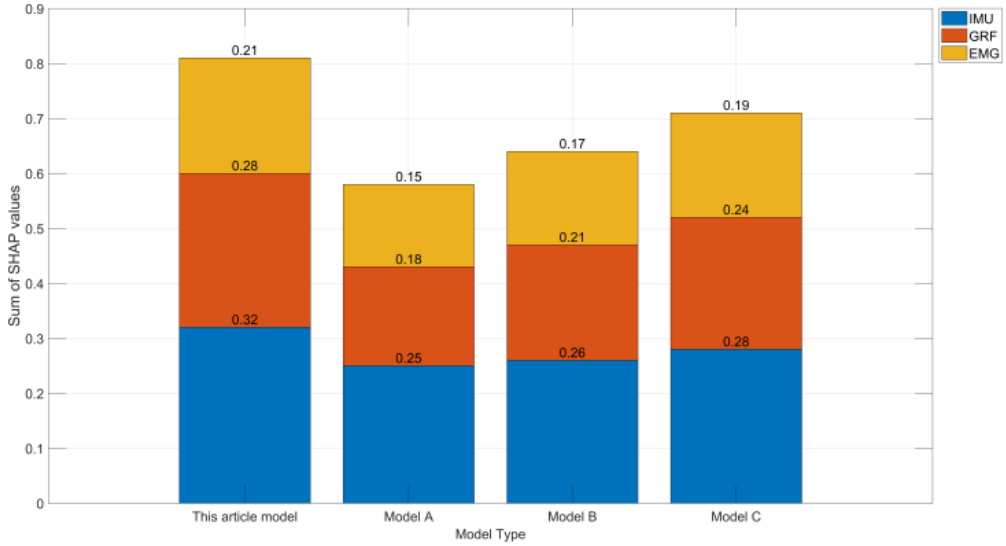

Figure 8: Distribution of SHAP value contribution of multi-source sensors

Fig. 8 shows the SHAP value contribution of this study and three comparative models on three sensor types: IMU, GRF, and EMG through a stacked bar chart. The X-axis is the model type, and the Y-axis is the sum of SHAP values. The data shows that the total column height of the model in this article is the highest, and the IMU part accounts for the largest proportion of 39.5%, indicating that it has the strongest dynamic screening ability for basketball-specific action characteristics; Model B has a total height of 0.64, and the IMU contribution of 0.26 is slightly higher than Model A but lower than the model in this article, reflecting that its multi-sensor fusion strategy has suboptimal recognition efficiency for key channels; Model C has a total height of 0.71, and the IMU contribution is close to the research method in this article compared with other models, but the GRF is 0.24, which is still significantly lower than 0.28 in this study, reflecting its insufficient capture of ground reaction force characteristics. The results verify the effectiveness of the TL framework for dynamic adjustment of sensor weights in long-term monitoring.

5.7 Accelerated aging test of signal drift

To study the sensor signal drift under high temperature and high humidity environment, a 48-hour accelerated aging test is carried out in an environment of 45°C/90%RH (Relative Humidity), and the sensor output signal drift is recorded. The signal drift results are shown in Fig. 9.

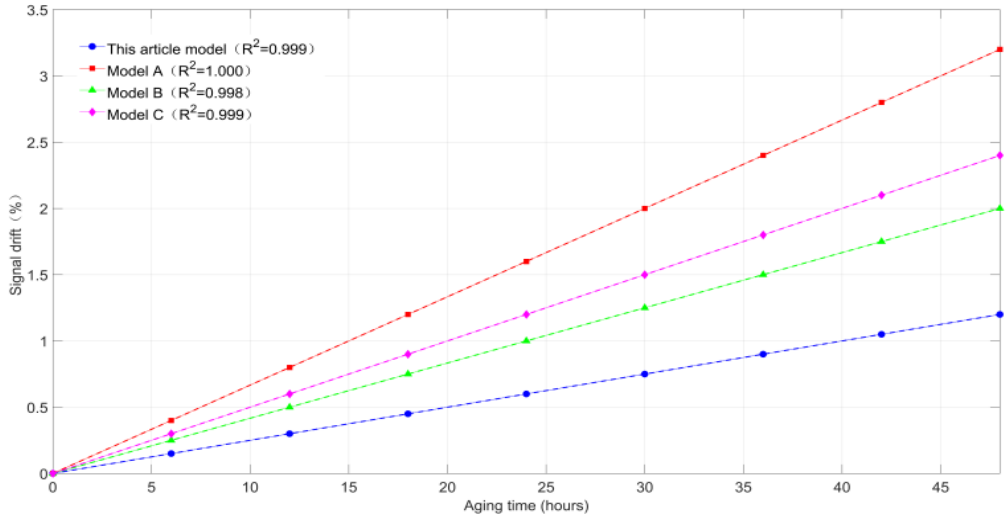

Figure 9: Device aging signal drift results

Fig. 9 illustrates the trend of signal drift variations across different models in accelerated aging tests. The horizontal axis denotes the aging duration, while the vertical axis indicates the signal drift. The scattered points and dotted lines of the four models correspond to the growth trajectory of their drift over time and the linear

fitting results. The data shows that the signal drift of this study gradually increases from the initial 0% to 1.2% in 48 hours, and the fitting slope is 0.025%/h; the drift of Model A surges from 0% to 3.20% in the same time, with a slope as high as 0.067%/h; Model B and Model C reach 2% (slope 0.042%/h) and 2.4% (slope 0.05%/h), respectively, which are significantly higher than the model of this study. At the 24-hour node, the drift of this study is 0.6%, while Models A/B/C reach 1.6%, 1%, and 1.2%, respectively, indicating that the signal stability of this study model in a high temperature and high humidity environment far exceeds that of the comparison model.

The underlying mechanism of this trend stems from the hardware combined with algorithm co-optimization adopted in this study: the environmental adaptability design based on the temperature and humidity impedance compensation model effectively suppresses the thermal drift of the sensor output signal, and the CNN-LSTM architecture of Model A amplifies the cumulative effect of signal noise due to the long sequence dependency problem. Model B relies on manual feature extraction and random forest classification. Although its signal drift growth rate is lower than that of Model A, it still fails to completely offset environmental interference due to the static nature of feature selection. Although the lightweight Transformer architecture of Model C performs better than Models A/B under electromagnetic interference, its drift rate is still higher than that of the study model in the aging test because the environmental compensation algorithm is not integrated. The results verify the comprehensive advantages of hardware and algorithm co-design in this study for long-term monitoring.

6 Conclusions

This study focuses on the fatigue monitoring needs of basketball players in Leshan during high-intensity training and constructs a collaborative framework based on multi-source sensor fusion and a spatiotemporal attention gated network. Through the joint optimization strategy of hardware and algorithm, it breaks through the limitations of traditional systems in real-time, individual adaptation, and environmental robustness. Aiming at the high dynamic characteristics of basketball special movements, a distributed sensor matrix including IMU, GRF, and EMG is designed. Based on the spatiotemporal feature extraction of 9-axis IMU and pressure insole, the dual-stream Transformer architecture is combined to dynamically screen key channels, and dynamic calibration of individual fatigue thresholds is achieved through TL. The experimental results show that the end-to-end delay of the system reaches 188ms; the AUC is improved by 9.4% compared with the CNN-LSTM model in 50 training cycles; the F1-score fluctuation of the guard and center is controlled at 0.05; the data packet loss rate does not exceed 0.25% in high temperature and high humidity environment, which verifies the advantages of the method in action-specific recognition and long-term monitoring stability. The study innovatively proposes a climate-adaptive wearable device with a gradient hydrophobic and hydrophilic composite structure; a spatiotemporal attention mechanism is constructed to achieve dynamic fusion of multi-source data, and the contribution weight of each sensor channel is analyzed through SHAP value; the individualized calibration framework based on TL reduces the model attenuation rate. The research provides a feasible technical solution for fatigue monitoring in basketball sports and also provides a methodological reference for the development of smart sports devices. Limitations and Future Work: This study focused on basketball players; generalizability to other sports requires further validation. Future work will explore integrating the system with coaching platforms for automated training plan adjustments.

Authorship contribution statement

Siyou WANG: Writing-Original draft preparation, Conceptualization, Supervision, Project administration.

Conflicts of interest

The authors state that they have no conflicts of interest related to this publication.

Author statement

All authors have reviewed and approved the manuscript, meeting the authorship requirements outlined earlier in this document, and each author believes it reflects honest work.

Ethical Approval

All authors have personally contributed significantly to the work that resulted in this paper and will assume public responsibility for its content.

Appendix: glossary of key terms and acronyms

IMU (Inertial Measurement Unit): A sensor that measures specific force, angular rate, and sometimes the magnetic field surrounding the device.

EMG (Electromyography): A technique for evaluating and recording the electrical activity produced by skeletal muscles.

ECG (Electrocardiography): A method for recording the electrical activity of the heart.

ML (Machine Learning): A subset of artificial intelligence that enables systems to learn from data without being explicitly programmed.

BiLSTM (Bidirectional Long Short-Term Memory): A type of recurrent neural network that processes data in both forward and backward directions to capture context from past and future states.

TL (Transfer Learning): A machine learning technique where a pre-trained model is fine-tuned on a new, related task.

AUC (Area Under the Curve): A performance metric for classification models, representing the probability that the model ranks a random positive instance higher than a random negative one.

F1-score: The harmonic means of precision and recall, providing a single score that balances both concerns.

References

[1] Y. Jiang, P. Malliaras, B. Chen, and D. Kulić, "Real-time forecasting of exercise-induced fatigue from wearable sensors," *Comput Biol Med*, Elsevier, vol. 148, p. 105905, 2022. https://doi.org/10.1016/j.compbiomed.2022.105905.

[2] A. Li, "Real-Time Athlete Fatigue Monitoring Using Fuzzy Decision Support Systems," *International Journal of Computational Intelligence Systems*, Springer, vol. 18, no. 1, p. 23, 2025. https://doi.org/10.1007/s44196-025-00732-8.

[3] A. Alzahrani and A. Ullah, "Advanced biomechanical analytics: Wearable technologies for precision health monitoring in sports performance," *Digit Health*, Sage Publications, vol. 10, p. 20552076241256744, 2024. https://doi.org/10.1177/20552076241256745.

[4] S. J. Ibáñez, P. López-Sierra, A. Lorenzo, and S. Feu, "Kinematic and neuromuscular ranges of external loading in professional basketball players during competition," *Applied Sciences*, MDPI, vol. 13, no. 21, p. 11936, 2023. https://doi.org/10.3390/app132111936.

[5] S. Pinelli, R. Zinno, A. Jòdar-Portas, A. Prats-Puig, R. Font-Lladó, and L. Bragonzoni, "Automated Detection of Change of Direction in Basketball Players Using Xsens Motion Tracking," *Sensors*, MDPI, vol. 25, no. 3, p. 942, 2025. https://doi.org/10.3390/s25030942.

[6] M. A. Ur Rahman Efti and M. I. Hosen, "3DOF Intelligent Rehabilitation Robot Design for Knee and Ankle," *Journal of Artificial Intelligence and System Modelling*, JAISM Bilijipub, vol. 1, no. 01, pp. 15–31, 2023. https://doi.org/10.22034/jaism.2023.423292.1005.

[7] Z. Yin, Z. Li, and H. Li, "Thermal radiation optical motion capture based on depth camera perception for basketball fatigue detection simulation," *Thermal Science and Engineering Progress*, Elsevier, vol. 56, p. 103072, 2024. https://doi.org/10.1016/j.tsep.2024.103072.

[8] S. J. Ibáñez, C. D. Gómez-Carmona, P. López-Sierra, and S. Feu, "Intensity thresholds for external workload demands in basketball: is individualization based on playing positions necessary?" *Sensors*, MDPI, vol. 24, no. 4, p. 1146, 2024. https://doi.org/10.3390/s24041146.

[9] D. I. Bourdas, A. K. Travlos, A. Souglis, D. C. Gofas, D. Stavropoulos, and P. Bakirtzoglou, "Basketball fatigue impact on kinematic parameters and 3-point shooting accuracy: insights across players' positions and cardiorespiratory fitness associations of high-level players," *Sports*, MDPI, vol. 12, no. 3, p. 63, 2024. https://doi.org/10.3390/sports12030063.

[10] J. Wang and H. Meng, "Sport fatigue monitoring and analyzing through multi-source sensors," *International Journal of Distributed Systems and Technologies (IJDST)*, IGI Global, vol. 14, no. 2, pp. 1–11, 2023. DOI: 10.4018/IJDST.317941.

[11] J. Burger, A.-S. Henze, T. Voit, R. Latzel, and O. Moser, "Athlete Monitoring Systems in Elite Men's Basketball: Challenges, Recommendations, and Future Perspectives," *Transl Sports Med*, Wiley Online Library, vol. 2024, no. 1, p. 6326566, 2024. https://doi.org/10.1155/2024/6326566.

[12] Z. Xie, "Fatigue monitoring and recognition during basketball sports via physiological signal analysis," *International Journal of Information System Modeling and Design (IJISMD)*, IGI Global, vol. 13, no. 2, pp. 1–11, 2022. DOI: 10.4018/IJISMD.313581.

[13] B. Song and P. Tuo, "Monitoring the physical condition of basketball players using IoT and blockchain," *Mobile information systems*, Wiley Online Library, vol. 2022, no. 1, p. 7657764, 2022. https://doi.org/10.1155/2022/7657764.

[14] M. Pernigoni *et al.*, "Match-related fatigue in basketball: A systematic review," *J Sports Sci*, Taylor & Francis, vol. 42, no. 18, pp. 1727–1758, 2024. https://doi.org/10.1080/02640414.2024.2409555.

[15] F. Li, D. Knjaz, and T. Rupčić, "Influence of fatigue on some kinematic parameters of basketball passing," *Int J Environ Res Public Health*, MDPI, vol. 18, no. 2, p. 700, 2021. https://doi.org/10.3390/ijerph18020700.

[16] Y. Hou, Z. Li, and H. Li, "Sensor based interactive digital entertainment and gamified training to alleviate basketball player fatigue," *Entertain Comput*, Elsevier, vol. 52, p. 100838, 2025. https://doi.org/10.1016/j.entcom.2024.100838.

[17] A. Biró, A. I. Cuesta-Vargas, and L. Szilágyi, "AI-assisted fatigue and stamina control for performance sports on IMU-generated multivariate times series datasets," *Sensors*, MDPI, vol. 24, no. 1, p. 132, 2024. https://doi.org/10.3390/s24010132.

[18] X. Wang and G. Dong, "Dynamic image simulation of thermal radiation based on optical sensor technology in basketball game simulation: Monitoring of muscle thermal energy consumption," *Thermal Science and Engineering Progress*, Elsevier, vol. 57, p. 103189, 2025. https://doi.org/10.1016/j.tsep.2024.103189.

[19] D. Mu, J. Wang, F. Li, W. Hu, and R. Chen, "Multilevel attention mechanism for motion fatigue recognition based on sEMG and ACC signal fusion," *PLoS One*, PLOS, vol. 19, no. 11, p. e0310035, 2024. https://doi.org/10.1371/journal.pone.0310035.

[20] Gai. X, "Application of flexible sensor multimodal data fusion system based on artificial

synapse and machine learning in athletic injury prevention and health monitoring," Discover Artificial Intelligence, vol. 5, no. 1, p. 31, 2025. https://doi.org/10.1007/s44163-025-00254-4.

[21] D. Miaoulis, I. Stivaros, and S. Koubias, "Developing a Novel Muscle Fatigue Index for Wireless sEMG Sensors: Metrics and Regression Models for Real-Time Monitoring," *Electronics (Basel)*, MDPI, vol. 14, no. 11, p. 2097, 2025. https://doi.org/10.3390/electronics14112097.